Ultracompact and low power optical switch based on silicon photonic crystals

Daryl M. Beggs[1,*], Thomas P. White[1], Liam O'Faolain[1] and Thomas F. Krauss[1]

[1]School of Physics and Astronomy, University of St Andrews, St Andrews, Fife, KY16 9SS, UK

[*]Corresponding author: daryl.beggs@st-andrews.ac.uk

Switching light is one of the most fundamental functions of an optical circuit. As such, optical switches are a major research topic in photonics and many types of switches have been realised. Most optical switches operate by imposing a phase shift between two sections of the device in order to direct light from one port to another, or to switch it on and off; the major constraint being that typical refractive index changes are very small. Conventional solutions address this issue by making long devices, thus increasing the footprint, or by using resonant enhancement, thus reducing the bandwidth. Here, we present a slow light enhanced optical switch that is thirty-six times shorter than a conventional device for the same refractive index change, and has a switching length of 5.2 μm.

OCIS codes: 130.4815, 130.5296, 230.4000, 230.5298.

A generic (non-mechanical) switch operates by interference between light that has propagated along two different paths or in two modes. Switching occurs when the relative path length of the light changes by half a wavelength, corresponding to a phase difference of π. Thus, for a device

of length L, the refractive index change required to switch from one state to another is given by $\Delta n\ L = \lambda/2$. Many switches are based on this principle; for example, using controlled birefringence, two-beam interference in a Mach-Zehnder interferometer (MZI), multi-mode interference in a directional coupler or Y-junction, or resonant enhancement in cavities [1].

Slow light in photonic crystal waveguides adds a degree of freedom to this equation. Slow light is similar to cavity enhancement, i.e. the optical path inside the device effectively increases while the physical size remains small [2], but it offers more bandwidth [3]. To highlight the capability of slow light enhancement, we refer to the MZI optical switches reported by Vlasov [4] and Gu [5] that operated with 8-10 times less power than a conventional switch of similar size.

The device presented here is based on a concept proposed by Yamamoto *et al* [6]. It exploits the fact that one of the two supermodes of the directional coupler has a low group velocity, which is the key design feature responsible for the short switching length. Figure 1 (top) shows the geometry; several sets of holes in the central section have been modified in order to tune the dispersion properties of the supermodes, and hence the coupling characteristics. Ridge waveguides at both ends of the device provide access to an interface region consisting of four rows of a slightly different photonic crystal structure, designed to give a dispersion relation that enables efficient injection of light into the device; this is especially important in the slow light regime, where large coupling losses can occur [7, 8]. The total size of the photonic crystal is approximately 9 μm × 9 μm, resulting in a footprint of less than 100 μm^2.

The dispersion of the central coupling region of the switch is engineered by controlling the sizes of three sets of holes, as illustrated in Fig. 1. The background lattice consists of holes of radius $r_0 = 0.34a$, where a = 430 nm is the lattice period. Between the waveguides, the holes

in the centre row have a radius $r_2 = 0.39a$, and in the rows immediately adjacent to the waveguide channel have $r_1 = 0.30a$. The holes in the second row of each waveguide also have the larger radius r_2. Figure 2 shows the dispersion curves of the supermodes in the coupling section (solid and dashed curves), calculated using MPB [9] with a sufficiently large supercell to minimise interactions between adjacent cells. The coupling length – the length at which the π phase difference required for switching occurs – is a function of the splitting of the two modes, $L_c = \pi/ (k_+ - k_-)$, where k_+ and k_- are the propagation constants of the two modes. The solid grey curve in Fig. 2 shows the variation in L_c with frequency for the designed coupler, directly calculated from the dispersion curves.

The key feature in Fig. 2 is the flat spot in the upper mode dispersion curve at normalised frequency $a/\lambda = 0.2736$, where the coupling length changes rapidly from more than $20a$ to approximately $5a$. A coupler with this geometry and a length $5a < L < 20a$ is thus expected to exhibit cross-coupling close to $a/\lambda = 0.2736$. Moreover, the rapid change in L_c results in a sharp transition from the bar- to the cross-state. The switch shown in Fig. 1 has a coupling section of length $L = 12a = 5.2$ μm, chosen to correspond to the middle of the transition region shown in Fig. 2. In practice, however, the first cross-coupling peak occurs slightly below the transition frequency due to an effective shortening of the coupling section caused by the modes requiring several lattice periods to become fully established upon entering from the input waveguides. We note that the switch proposed in [6] was designed to operate on either side of the transition region in order to maximise the bandwidth, whereas the present design sacrifices some bandwidth in order to reduce the index change required for switching.

The devices were fabricated using the same process as in [10], except that the patterns were generated on our Raith Elphy Plus/LEO 1530 electron-beam lithography system.

Controlling the hole size is the most critical aspect of the design. To this end, we fabricate reference W1 waveguides with each of the three hole sizes used in the coupler. By measuring the cut-off wavelength of each waveguide, we can infer the hole size to an accuracy of approximately 1%; better than by SEM inspection. This feedback loop is used to optimize the lithography parameters and monitor the hole sizes in the fabricated devices. While there is some variation in the fabricated hole size with processing conditions, the relative sizes do not change significantly.

Devices are characterised in an end-fire set-up, using a broadband LED source. For a proof-of-principle experiment, switching via the thermo-optic effect is demonstrated by heating the optical stage supporting the device. At near-infrared wavelengths, the thermo-optic effect in silicon will produce a change in refractive index of $\Delta n = 1.8 \times 10^{-4}\ \mathrm{K}^{-1}$ [11].

Figures 3 (*a*) and (*b*) show the transmission spectra of both the bar (dashed black curve) and cross (solid black curve) ports of the directional coupler, normalized to the transmission of a typical 3 μm wide waveguide, for two different temperatures: 23°C (*a*) and 45°C (*b*). The on-chip insertion loss of the switch is approximately 1 dB, which is comparable to that of a single W1 photonic crystal waveguide. The extinction ratio, defined as the ratio of power in the bar port to the power in the cross port, is also shown (top) for both 23°C (solid line) and 45°C (dashed line). The vertical grey line indicates the operating wavelength of the switch, and taking Fig. 3 as a whole illustrates the operational principle.

In the initial state (Fig. 3*a*), output is in the bar port with an extinction ratio of –20.0 dB. By changing the refractive index of the silicon – we use the thermo-optic effect, but it could be any other physical mechanism – the spectrum shifts in wavelength whilst maintaining its shape (provided $\Delta n << n$), switching the output into the cross port (Fig. 3*b*), with an extinction ratio of

12.0 dB. Hence, switching is achieved with a discrimination ratio exceeding 30 dB for an index change as small as 4.2×10^{-3}.

Figure 4 shows the power in the bar and cross ports of the switch at the operating wavelength of 1575 nm as a function of temperature. As expected from Fig. 3, the signal transfers from the bar to the cross port for a temperature change of approximately 20°C. The two inset photos show the output facet of the device at 23 and 45°C, respectively, and almost perfect power transfer is observed.

Also shown in Fig. 3(*a*) and (*b*) are spectra calculated using a three-dimensional finite-difference time-domain (FDTD) method. The simulation domain included short lengths of ridge waveguide at either end of the device, but did not include the s-bends or the extended access waveguides used in the experimental measurements. The numerical results presented in this paper were calculated for $r_0 = 0.335a$ and a membrane thickness of 225nm – values chosen to give the best fit to the measured data while staying within the experimental uncertainties. The excellent agreement between experimental and theoretical spectra attests not only to the high fabrication quality of the devices, but also to the accuracy with which the hole sizes are controlled. Maintaining such control gives further scope for dispersion engineering in photonic crystals for other applications [12, 13].

The switching energy is an important parameter and is largely a function of the device size and refractive index change required. Resonant cavity based switches can provide ultra-low switching energy given their small modal volumes and sharp spectral responses. For example, switching in high-Q nanocavities has recently been reported for energies of 0.2-0.3 pJ [14]; however, the high quality factor of the resonance also reduces the available bandwidth considerably. In contrast, the MZI modulator demonstrated by Vlasov *et al* [4] offers more

bandwidth, but also displays a higher switching energy of 200 pJ, which is comparable to our device. The volume of silicon that contains the super-modes of the directional coupler is approximately half that of the airbridge, i.e. 4.6×10^{-18} m^3 (4.6 μm^3), and therefore its heat capacity is approximately 8 pJ/K. Since switching occurs over a temperature difference of 23 K, the switching energy is estimated as 200 pJ.

Returning to the generic switching condition ($\Delta n\ L = \lambda/2$) allows us to estimate the enhancement afforded by the peculiar dispersion curves of the photonic crystal coupler (Fig. 2). For a conventional switch, the $\Delta n\ L$ product is simply half the wavelength, i.e. 1574/2 = 787 nm. For our switch, the switching length is $12a$ = 5.2 μm and the refractive index change is $\Delta n = 4.2 \times 10^{-3}$, yielding a $\Delta n\ L$ product of 22 nm, which is 36 times smaller than that of the conventional device. The penalty of this enhancement is a reduced bandwidth – here limited by the smaller of the ± 5 dB extinction ratio widths (i.e. 1.2 nm) – and yet the observed bandwidth is sufficient to accommodate optical signals of order 100 GHz. As discussed above, the design is flexible and allows the choice of different operating points to suit individual requirements, for example to match the lower refractive index changes available with electronic tuning. Overall, we have demonstrated a truly microscale optical switch that breaks the $\Delta n\ L$ product of conventional switches by a factor of 36.

Acknowledgements

The work was funded through the EU FP6-FET "Splash" project and we acknowledge the Nanostructuring Platform of EU FP6-NoE "epixnet" for technical support. T. P. White is supported by an 1851 Royal Commission Research Fellowship.

References

1. "Optical Switching", El-Bawab, Tarek S. 2006 ISBN: 978-0-387-26141-6.
2. T. F. Krauss, J. Phys. D: Appl. Phys. **40** (9) 2666-2670 (2007).
3. M. D. Settle, R. J. P. Engelen, M. Salib, A. Michaeli, L. Kuipers, and T. F. Krauss, Opt. Express **15** (1) 219-226 (2007).
4. Y. A. Vlasov, M. O'Boyle, H. F. Hamann, S. J. McNab, Nature **438** 65-69 (2005).
5. L. Gu, W. Jiang, X. Chen, L. Wang, and R. T. Chen, Appl. Phys. Lett. **90** 071105 (2007).
6. N. Yamamoto, T. Ogawa, and K. Komori, Opt. Express **14** (3) 1223-1229 (2006).
7. Y. A. Vlasov and S. J. McNab, Opt. Lett. **31** (1) 50-52 (2006).
8. J. P. Hugonin, P. Lalanne, T. P. White, and T. F. Krauss, Opt. Lett. **32** (18), 2638-2640 (2007).
9. S. G. Johnson and J. D. Joannopoulos, Optics Express **8** (3) 173-190 (2000).
10. L. O'Faolain, X. Yuan, D. McIntyre, S. Thoms, H. Chong, R. M. De la Rue, and T. F. Krauss, Electron. Lett. **42** (25) 1454-1455 (2006).
11. J. A. McCaulley, V. M. Donnelly, M. Vernon, and I. Taha, Phys. Rev. B **49** (11) 7408-7417 (1994).
12. D. Mori, and T. Baba, Opt. Express **13** (23) 9398-9408 (2005).
13. Yu. Petrov and M. Eich, IEEE Journal of Selected Areas in Communications **23** (7) 1396-1401 (2006).

14. M. Notomi, A. Shinya, S. Mitsugi, G. Kira, E. Kuramochi, T. Tanabe, Opt. Express **13** (7) 2678-2687 (2005).

References (with titles)

1. 'Optical Switching", El-Bawab, Tarek S. 2006 ISBN: 978-0-387-26141-6.

2. T. F. Krauss, "Slow light in photonic crystal waveguides," J. Phys. D: Appl. Phys. **40** (9) 2666-2670 (2007).

3. M. D. Settle, R. J. P. Engelen, M. Salib, A. Michaeli, L. Kuipers, and T. F. Krauss, "Flatband slow light in photonic crystals featuring spatial pulse compression and terahertz bandwidth," Opt. Express **15** (1) 219-226 (2007).

4. Y. A. Vlasov, M. O'Boyle, H. F. Hamann, S. J. McNab, "Active control of slow light on a chip with photonic crystal waveguides," Nature **438** 65-69 (2005).

5. L. Gu, W. Jiang, X. Chen, L. Wang, and R. T. Chen, "High speed silicon photonic crystal waveguide modulator for low voltage operation," Appl. Phys. Lett. **90** 071105 (2007).

6. N. Yamamoto, T. Ogawa, and K. Komori, "Photonic crystal directional coupler switch with small switching length and wide bandwidth," Opt. Express **14** (3) 1223-1229 (2006).

7. Y. A. Vlasov and S. J. McNab, "Coupling into the slow light mode in slab-type photonic crystal waveguides," Opt. Lett. **31** (1) 50-52 (2006).

8. J. P. Hugonin, P. Lalanne, T. P. White, and T. F. Krauss, "Coupling into slow-mode photonic crystal waveguides,"Opt. Lett. **32** (18), 2638-2640 (2007).

9. S. G. Johnson and J. D. Joannopoulos, "Block-iterative frequency domain methods for Maxwell's equations in a planewave basis", Optics Express **8** (3) 173-190 (2000).

10. L. O'Faolain, X. Yuan, D. McIntyre, S. Thoms, H. Chong, R. M. De la Rue, and T. F. Krauss, "Low-loss propagation in photonic crystal waveguides," Electron. Lett. **42** (25) 1454-1455 (2006).

11. J. A. McCaulley, V. M. Donnelly, M. Vernon, and I. Taha, "Temperature dependence of the near-infrared refractive index of silicon, gallium arsenide, and indium phosphide," Phys. Rev. B **49** (11) 7408-7417 (1994).

12. D. Mori, and T. Baba, "Wideband and low dispersion slow light by chirped photonic crystal coupled waveguide," Opt. Express **13** (23) 9398-9408 (2005).

13. Yu. Petrov and M. Eich, "Dispersion compensation with photonic crystal line-defect waveguides," IEEE Journal of Selected Areas in Communications **23** (7) 1396-1401 (2006).

14. M. Notomi, A. Shinya, S. Mitsugi, G. Kira, E. Kuramochi, T. Tanabe, "Optical bistable switching action of Si high-Q photonic-crystal nanocavities", Opt. Express **13** (7) 2678-2687 (2005).

Figure Captions

Figure 1 Scanning electron micrographs of the directional coupler switch. Top: the coupler consists of two photonic crystal waveguides made up of three regions: the central directional coupler region of length 12*a*, and input and output regions each of length 4*a*. Bottom left: overview of the structures: s-bends are used in order to prevent interactions between the access waveguides and provide sufficient spatial separation at the facets to observe each output port. Bottom right: detail of the three hole sizes used to engineer the dispersion of the photonic crystal waveguides.

Figure 2 Dispersion curves of the upper (solid black) and lower (dashed) modes of the central section of the device (bottom axis). The corresponding coupling length is shown as a grey curve (top axis). The dotted lines indicate the frequency at which cross-coupling occurs in the switch of length 12*a*.

Figure 3 Spectral response of the device at 23°C (*a*) and 45°C (*b*). (*a*) and (*b*) show the measured transmission spectra of light from the bar-port (dashed black curve) and the cross-port (solid black curve). Also shown are numerical results calculated using a 3D FDTD method (grey squares and curves). The measured extinction ratio is also shown (top) for 23°C (solid line) and 45°C (dashed line). The vertical grey line indicates the operating wavelength of the switch.

Figure 4 Transmission through the bar-port (open squares) and cross-port (closed squares) as a function of temperature. The corresponding refractive index of silicon is shown on the top axis. The left and right insets show images of the end facet for the bar and cross output states, respectively.

Figure 1

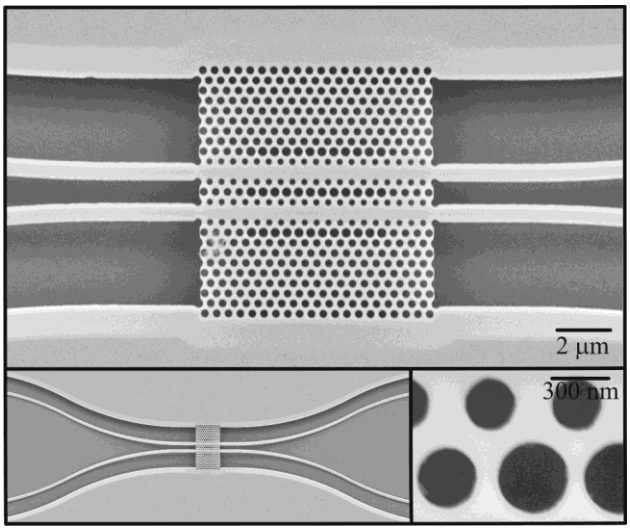

Figure 2

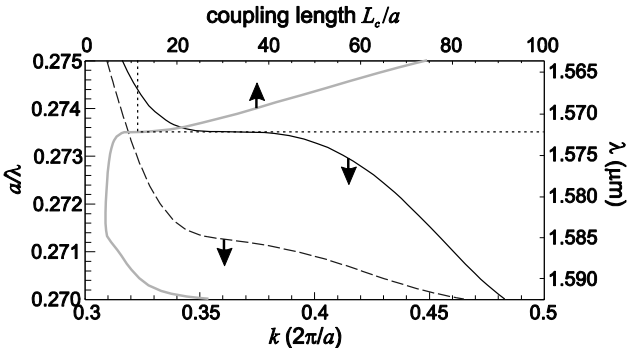

Figure 3

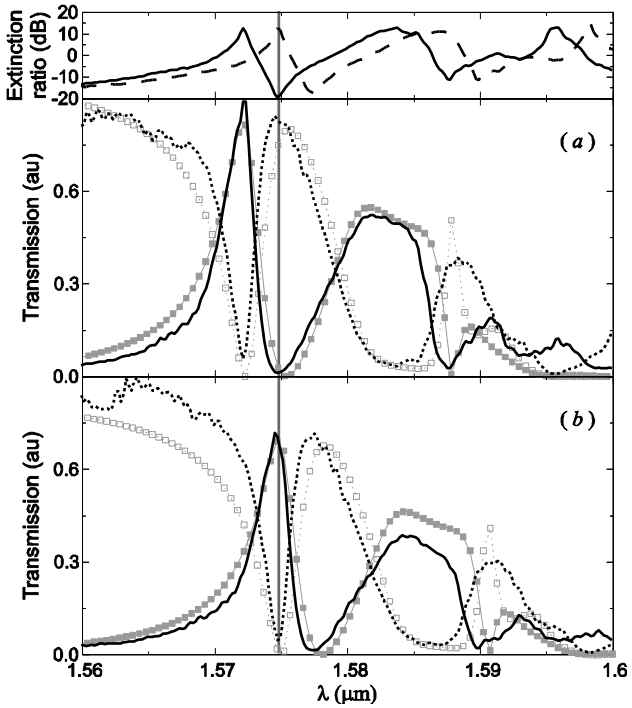

Figure 4